Title

Non-iterative method for constructing valence antibonding molecular orbitals and a molecule-adapted minimum basis

Journal

The Journal of Chemical Physics, 157(9)

ISSN

0021-9606

Authors

Aldossary, Abdulrahman
Head-Gordon, Martin

Publication Date

2022-09-07

DOI

10.1063/5.0095443

Non-iterative Method for Constructing Valence Antibonding Molecular Orbitals and a Molecule-adapted Minimum Basis.

Abdulrahman Aldossary and Martin Head-Gordon*

Pitzer Center for Theoretical Chemistry, Department of Chemistry, University of California, Berkeley CA 94720, USA

E-mail: mhg@cchem.berkeley.edu

Abstract

While bonding molecular orbitals exhibit constructive interference relative to atomic orbitals, antibonding orbitals show destructive interference. When full localization of occupied orbitals into bonds is possible, bonding and antibonding orbitals exist in 1:1 correspondence with each other. Antibonding orbitals play an important role in chemistry because they are frontier orbitals that determine orbital interactions, as well as much of the response of the bonding orbital to perturbations. In this work, we present an efficient method to construct antibonding orbitals by finding the orbital that yields the maximum opposite spin pair correlation amplitude in second order perturbation theory (AB2) and compare it with other techniques with increasing the size of the basis set. We conclude the AB2 antibonding orbitals are a more robust alternative to the Sano orbitals as initial guesses for valence bond calculations, due to having a useful basis set limit. The AB2 orbitals are also useful for efficiently constructing an active space, and work as good initial guesses for valence excited states. In addition, when combined with the localized occupied orbitals, and relocalized, the result is a set of molecule-adapted minimal basis functions that is built without any reference to atomic orbitals of the free atom. As examples, they are applied to population analysis of halogenated methane derivatives, H-Be-Cl, and SF_6 where they show some advantages relative to good alternative methods.

1 Introduction

Virtual orbitals are important in chemistry as they play a central role in molecular orbital theory. From a computational standpoint, orbital mixing between occupieds and virtuals determines the optimal occupied orbitals in mean-field Hartree-Fock theory[1–3] and Kohn-Sham density functional theory.[4–7] In wavefunction theory, electron correlation is typically described by amplitudes such as the pair correlations describing the simultaneous promotion of two electrons from occupied to virtual orbitals. The virtual orbitals span the unoccupied space, and the choice of representation is important. Canonical virtual orbitals are delocalized levels that are appropriate for electron attachment. Localized virtuals, such as the redundant non-orthogonal basis of atomic orbitals projected into the virtual space,[8,9] permit development of efficient local correlation methods, because the amplitude tensors describing correlation become sparse.[10] Other prescriptions for localized orthogonal virtuals exist,[11–13] as well as proposals to form sets of virtuals that are specifically optimized for correlations that involve a given occupied level, as will be discussed below.

The virtual orbitals span the entire unoccupied space, which can be contrasted with the intuitive notion of antibonding orbitals that exist in 1:1 correspondence with bonding orbitals. The 1:1 correspondence is evident from constructive and destructive interference of a pair of 1s-type functions on two hydrogen atoms in H_2:

$$\sigma = N\left(1s_A + 1s_B\right) \tag{1}$$

$$\sigma^\star = N^\star\left(1s_A - 1s_B\right) \tag{2}$$

Antibonding orbitals themselves play a central role in describing chemical reactivity[14–19] of one molecule with another through donor-acceptor interactions between a high-lying occupied of one species with a low-lying antibonding orbital of the other. Frontier orbital theory is constructed on these ideas. Antibonding orbitals also play an important role in describing strong electron correlations. A simple example is the stretching of the H-H bond which leads, in a minimal basis, to a strong increases in the amplitude for $\sigma\bar{\sigma} \rightarrow \sigma^\star\bar{\sigma^\star}$ excitation which breaks the bond.

While the antibonding orbitals are intuitive,[16–18,20] it is nonetheless not routine to extract them from modern quantum chemistry calculations performed in extended basis sets, which return canonical orbitals. By contrast, in a minimal basis description of hydrocarbons, the space of antibonding orbitals is naturally spanned by the canonical virtual orbitals. In larger basis sets however, different methods have been developed to extract the antibonding orbitals, often by relying on projection back onto some chosen minimal basis,[13,21–25] typi-

cally a tabulated one for a specific free-atom Hartree-Fock energy eigenstate. For example, Schmidt et. al. found antibonding orbitals by performing an SVD of the overlap between the virtual orbitals and a minimal basis to produce valence virtual orbitals.[13] Some methods have been developed to produce a minimal basis specifically adapted to a molecular environment,[26,27] but those are non-linear optimization procedures that are often iterative and costly. One famous method that does not rely on a reference minimal basis is the Natural Bond Orbital (NBO) procedure,[14,15] where the density matrix coupling between multiple atom-tagged orbitals is utilized to produce bonding and anti-bonding orbitals. However, atom tagging of basis functions plays a critical role in the NBO procedure – in fact, the standard NBO method is specific to atom-centered orbital (AO) basis calculations. Few methods cut the umbilical cord to the minimal basis in producing antibonding orbitals. Aside from the Sano antibonding orbitals[28] (discussed below), Foster and Boys[29] suggested oscillator orbitals which are virtual orbitals with the maximum dipole from localized occupied orbitals.

Local correlation has been intensively studied,[8,9,25,30–38] leading to the conclusion that dynamic correlation can be well approximated using domains of localized virtual orbitals that are in the same spatial region as a localized occupied orbital.[8,9] This reduces the 4th rank tensor of pair correlation amplitudes to an asymptotically linear number of significant elements. Nevertheless, all virtual orbitals are required for post-SCF methods such as coupled cluster theory that recover dynamic correlation, rather than just the much smaller set of valence virtual orbitals. By contrast, static or strong correlation, resides mostly in the valence virtuals (i.e. the antibonding orbitals). Thus complete active space (CAS) methods that seek to describe strong correlation require only a description of the valence virtuals. Methods in this class include CASSCF,[2,39–42] spin-coupled valence bond (VB),[43–46] and approximations such as generalized valence bond (GVB),[47] coupled cluster valence bond (CCVB),[48–50] etc. CAS, GVB and CCVB methods thus need an initial guess for the antibonding orbitals. We do note that the orbitals associated with key amplitudes for strong correlation are not necessarily spatially localized.[51–54]

One method used to obtain initial guess antibonding orbitals is the so-called Sano procedure.[28] In brief, after localizing a set of occupied orbitals using standard methods,[12,55–57] the Sano procedure finds the virtual orbital that has maximum exchange interaction with each given localized occupied orbital. The idea of maximizing exchange is very old[58,59] and comes from its predecessor, the modified virtual orbitals[60,61] (note that modified virtual orbitals have been since used to refer to any non-canonical set of virtual orbitals[62]). The resulting orbitals are symmetrically orthogonalized to yield a set of valence antibonding orbitals. This method has worked quite well for GVB-PP and CCVB calculations in moderately sized

basis sets.[49–51,63,64] In this work we will show that the Sano procedure shows undesirable behavior with increasing the size of the AO basis set. This motivates the need for a better behaved alternative. We suggest that finding the antibonding orbital which gives the largest first order perturbation amplitude for exciting an electron pair from a given bonding orbital is a suitable alternative. A range of numerical results confirm this to be the case. These antibonding orbitals can be viewed as a specific instance of orbital specific virtuals.[30–32]

2 Theory

2.1 Defining the set of antibonding orbitals

Solving the mean field Hartree-Fock (HF) equation self consistently gives the lowest energy single Slater determinant electronic wave function. To solve the many-body problem, one needs to include the missing correlation energy.[65] Second order Møller-Plesset (MP2) perturbation theory[66,67] offers a useful and computationally inexpensive approximation to treat the correlation yielding the following expression in the case of restricted HF orbitals:

$$E^{(2)} = \sum_{ij}^{occ} \sum_{ab}^{virt} \tau_{ij}^{ab} \, (ia|jb) \tag{3}$$

where

$$\tau_{ij}^{ab} = \frac{2(ia|jb) - (ib|ja)}{\epsilon_i + \epsilon_j - \epsilon_a - \epsilon_b} \tag{4}$$

This expression folds together contributions from the correlation of two electrons of opposite spin (OS), with amplitudes:

$$t_{ij}^{ab} = \frac{(ia|jb)}{\epsilon_i + \epsilon_j - \epsilon_a - \epsilon_b} \tag{5}$$

together with the contribution of correlations of electrons with the same spin. The two-electron repulsion integrals (ERIs) over spatial orbitals describing the interaction of each occupied with each virtual are:

$$(ia|jb) = \int d\mathbf{r}_1 \phi_i(\mathbf{r}_1)\phi_a(\mathbf{r}_1) \int d\mathbf{r}_2 r_{12}^{-1} \phi_j(\mathbf{r}_2)\phi_b(\mathbf{r}_2) \tag{6}$$

Let us collect the ERIs associated with occupied orbital i into the symmetric matrix $\mathbf{K}^i$, where:

$$K_{ab}^i = (ia|ib) \tag{7}$$

$\mathbf{K}^i$ is positive semi-definite, and thus the eigenvector belonging to its largest eigenvalue will

correspond to the virtual level with the strongest exchange interaction with occupied level i. That is the Sano prescription[28] for finding the antibonding orbital associated with i.

We can likewise define a matrix of second order pair correlation amplitudes, $\mathbf{T}^i$, associated with a given occupied orbital:

$$T^i_{ab} = t^{ab}_{ii} \tag{8}$$

This matrix is negative semi-definite since the denominators are negative for the ground state determinant. We can therefore find the largest OS pair-correlation amplitude as the lowest eigenvalue, $t^i_{\max}$ of $\mathbf{T}^i$, and the associated virtual orbital, $|i^*\rangle = \sum_a |a\rangle\, c_{ai^*}$ is the eigenvector, with expansion coefficients c_{ai^*} in the original virtual basis:

$$\sum_b T^i_{ab} c_{bi^*} = t^i_{\max} c_{ai^*} \tag{9}$$

Upon repeating for each occupied level, most naturally in a localized representation, and using similar arguments to Kapuy's zeroth in the Fock and 2nd order in correlation approximation,[68,69] we suggest that this is an appropriate non-iterative way to find a set of antibonding orbitals in 1:1 correspondence with the bonding orbitals. This approach may be contrasted with Sano's suggestion to obtain the virtual orbital with maximum repulsion from the bonding orbital by solving the eigenvalue problem for each orbital using $\mathbf{K}^i$ rather than $\mathbf{T}^i$. Inclusion of orbital denominators in Eq. 9 provides a clear physical meaning of the antibonding orbital as having strongest pair correlation amplitude with its parent bonding orbital. As will be demonstrated numerically later, this property also dramatically improves basis set convergence relative to the Sano definition.

We will refer to these virtual orbitals as "second order antibonding" (AB2) MOs to emphasize their second order origins, and their 1:1 correspondence with bonding MOs. In terms of existing literature, the AB2s are directly related to the "orbital-specific virtual" (OSV) orbitals[30,31] that are sometimes used to evaluate the correlation energy. Each AB2 orbital is the most important OSV for a given localized bonding orbital. Of course the reason for selecting the amplitudes associated with MP2 is computational efficiency. The exact limit of this procedure would be to diagonalize the corresponding exact (i.e. from Full CI) doubles amplitudes; T^i_{ab}, via Eq. 9.

A closely related alternative that has some advantages over Eq. 9 above is to define the space of valence antibonding orbitals from the virtual-virtual block of the MP2 one-particle density matrix:[70,71]

$$P_{ab} = \sum_{ijc} t^{ac}_{ij} t^{bc}_{ij} \tag{10}$$

Upon diagonalizing, the $(M - O)$ eigenvectors with largest occupation numbers span the

valence antibonding orbital space, and, together with the occupied space, complete the span of a molecule-adapted minimal basis. Localization of these valence virtual orbitals will then yield an alternative to the localized virtuals above. The advantage of this approach is for cases where there is no simple 1:1 mapping between bonding and antibonding orbitals, as discussed more later.

The virtual orbitals obtained this way are the valence subset of the "frozen natural orbitals" (FNO),[70,71] and we emphasize that they are not generally localized in contrast to the AB2 MOs. They are close to the virtual natural orbitals associated with P^{MP2} as defined by the gradient of the MP2 energy,[72–74] with the caveat that only the virtual-virtual block is diagonalized.

2.2 Population analysis using the effective minimal basis

Finding a suitable set of antibonding orbitals provides the missing part of the valence space not spanned by the occupied orbitals. Thus the union of the occupied space and the space of antibonding orbitals spans the space of an effective minimal basis. It is well accepted that full valence CASSCF wavefunction is spanned by an effective minimal basis within the molecule for this reason.[39,40] Accordingly, localizing the union of the occupied orbitals with the antibonding orbitals reveals a set of molecule-adapted atomic orbitals (MAOs):[75,76]

$$\mathbf{C}_{\mathrm{MAO}} = \{\mathbf{C}_{\text{non-bonding}}\} \oplus \{\mathrm{Localize}(\mathbf{C}_{\text{bonding}} \oplus \mathbf{C}_{\text{antibonding}})\} \tag{11}$$

For a given pair of well-localized bonding and antibonding orbitals (say σ and σ^*), this procedure amounts to inverting Eqs. 2 to discover the corresponding MAOs even though we may be using a very extended basis, or even a non-atom-centered basis, such as plane waves or a real-space grid, to perform the calculations.

The resulting MAOs, $\boldsymbol{\chi}$ are thus expressed in terms of the AO's, $\boldsymbol{\omega}$, as $\boldsymbol{\chi} = \boldsymbol{\omega}\mathbf{C}_{\mathrm{MAO}}$. The MAOs are orthogonal, and typically localize onto atoms. The MAOs exactly span the space of the occupied orbitals, and can be used for population analysis among other things.[26,40,77–83] Let us denote p as an MAO label for χ_p, which is centered at $\mathbf{r}_p = \langle\chi_p|\mathbf{r}|\chi_p\rangle$. Using A, B as atom labels, and given that the density matrix in the MAO basis is $\mathbf{P}^{\mathrm{MAO}} = \mathbf{C}_{\mathrm{MAO}}^{\dagger}\mathbf{SPSC}_{\mathrm{MAO}}$, one can make a population analysis as follows:

$$p \in A \iff |\mathbf{r}_p - \mathbf{R}_A| = \min_B(|\mathbf{r}_p - \mathbf{R}_B|) \tag{12}$$

$$Q^A = Z^A - \sum_{p\in A} P_{pp}^{\mathrm{MAO}} \tag{13}$$

where Q^A and Z^A are the atomic charge and the nuclear charge, respectively. Such a population analysis has no dependence on atom-tagging of the underlying basis, and does not rely upon a reference minimal basis. Therefore it generalizes nicely to plane wave basis and real space methods. If the orbitals are unrestricted, we construct antibonding pairs and the MAOs for the alpha and beta spin spaces independently.

This approach to generating an MAO representation does have some limitations. First, it assumes that there is a 1:1 mapping between bonding and antibonding orbitals. One class of exceptions can be found in electron deficient molecules (e.g. LiH will not recover 2p-like orbitals on Li, and BH_3 will not recover a $2p_z$ orbital on B). Such species can be said to have "virtual lone pairs", whose identification is a problem that we shall not address here. A second class of exceptions lie in species such as cyclopentadiene anion, where there are 3 semi-localized π occupied orbitals, but the valence space only admits 2 antibonding orbitals. Thirdly, in symmetric systems with multiple Lewis structures (e.g. C_6H_6), the MAOs will derive from localized bond and antibonding orbitals corresponding to a single Lewis structure and may not reflect the indistinguishability of the atoms. Broadly, we can say that this MAO approach is readily applicable to neutral molecules with a single dominant Lewis structure.

2.3 Implementation details

Computational efficiency is very important for quantum chemistry in order treat molecules that are as large as possible for given computational resources (computer speed, memory size, etc). Our AB2 implementation uses exact 4-center integrals in a basis of Gaussian-type atomic orbitals (other alternatives such as using auxiliary basis expansions can also be readily implemented). Each step with its computational complexity is shown in Fig. 1. Note that for the figure and the discussion here we use O, V, and N for the number of bonding orbitals, virtual orbitals, and AO basis functions, respectively. We start by making a pseudo-density $\mathbf{P}^i = \mathbf{C}_i\mathbf{C}_i^\dagger$ for each bonding orbital, i. To generate the two-electron integrals $(\mu\nu|\lambda\sigma)$, Q-Chem[84] only generates significant $\mu\nu$ (i.e. AO basis) pairs to some target numerical cutoff, yielding a total that we term as $(NN)_{\text{cut}}$. $(NN)_{\text{cut}}$ scales quadratically (i.e. $(NN)_{\text{cut}} \approx N^2$) for small systems but approaches linear scaling (i.e. $(NN)_{\text{cut}} \propto N$) in the limit of large system size. The integrals are made and contracted on-the-fly with the bonding orbitals' pseudo-densities to make bonding-specific exchange integrals $K^i_{\mu\nu}$ with compute effort scaling as $\mathcal{O}(O(NN)^2_{\text{cut}})$. The $K^i_{\mu\nu}$ matrices are then transformed into the virtual space as K^i_{ab} in Eq. 7 with compute cost scaling as $\mathcal{O}(OVN^2 + OV^2N)$. Asymptotically this is the dominant step in this method unless more careful thresholding is considered.[85] Then, we divide by the appropriate denominator to get T^i_{ab} in Eq. 8 (with $\mathcal{O}(OV^2)$ effort). Lastly, we diagonalize

$\mathbf{T}^i$ for each bonding orbital to get the AB2 antibonding orbitals as in Eq. 9 with $\mathcal{O}(OV^3)$ effort. Note that the last step can in principle be made $\mathcal{O}(OV^2)$ since we are only solving for the eigenvector with the largest amplitude in each matrix. We can contrast this procedure with the modified FNO approach which has a dominant computational step that scales as the 5^{th} power of molecule size: constructing P_{ab} in Eq. 10 with complexity of $\mathcal{O}(O^2V^3)$.

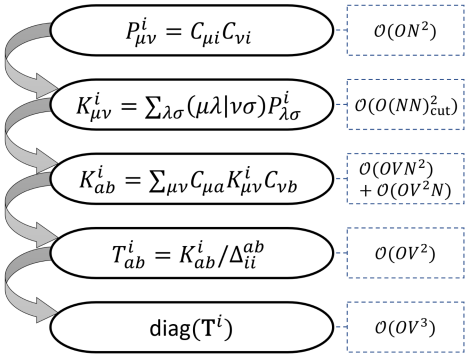

Figure 1: A chart illustrating the mathematical steps needed to construct AB2 orbitals with the appropriate computational complexity for each step indicated. Here, O, V, N, and $(NN)_{\text{cut}}$ refer to the number of occupied orbitals, virtual orbitals, AO basis functions, and significant AO pairs, respectively.

One reason for the efficiency of the AB2 approach compared to FNO comes from focusing on the bonding orbitals one at a time rather than the whole occupied space at once. It is then important to start by localizing the occupied space, which is known to be a cubic scaling iterative procedure for e.g. the Boys and Pipek-Mezey localization measures.[86,87] Then, one must also distinguish between localized orbitals with different character: specifically core, bonding, and non-bonding, e.g. lone pairs. Our implementation uses an automatic bonding detection option that runs before AB2. The detection process is simply determined by Pipek's delocalization measure[88] on Mulliken charges, where measures amounting to 1 indicate an orbital localized on an atom (core or non-bonding) and measures around 2 correspond to orbitals split between two atoms.

2.4 Computational details

All methods discussed here were implemented in a developer version of Q-Chem 5.[84] The geometries used for molecular calculations were optimized at the ωB97X-D/def2-TZVPD level of theory. All geometries are included in the Supplementary Material (SI).

3 Results and discussion

We will compare different approaches to generating effective antibonding orbitals: in particular we are interested in whether the second order antibonding (AB2) MOs significantly improve upon the Sano antibonding orbitals, as measured by usage-relevant metrics obtained from a set of numerical experiments. We will first examine orbital plots, orbital energies, and orbital variances. We then test the applicability of Sano and AB2 MOs to several valence correlation methods: coupled cluster valence bond (CCVB),[49,50] complete active space configuration interaction (CASCI),[89–92] and complete active space self-consistent field (CASSCF).[39–42] Next, we look into their uses for describing valence excited states. For basis set, we are using the Dunning basis set family[93] and Ahlrichs.[94] These are available in Q-Chem 5.3 with an automated detection of bonding orbitals.

3.1 Orbitals, orbital Energy, and orbital variance

We start by looking at the σ^* orbital of H_2, as shown in Fig. 2, evaluated by the Sano procedure, the AB2 approach, and CAS(2,2) (performed as 1-pair perfect pairing). It is visually clear that the Sano σ^* orbital is contracting as the basis set is improved. Fig. 3 displays the orbital energy (diagonal matrix element of the Fock operator) and the variance ($\langle r^2 \rangle - \langle \mathbf{r} \rangle^2$) of the σ bonding orbital, and the Sano and AB2 models of the antibonding orbital. The variance confirms that the size of the Sano σ^*-orbital contracts with basis size, while its orbital energy increases (reflecting increasing electron confinement) unsatisfactorily. By contrast the behavior of the AB2 orbital is very close to the bonding orbital, with pleasing stability in both energy and variance as the basis set is converged towards completeness. The stark difference is due to Sano orbitals including high energy orbitals to maximize the exchange interaction whereas AB2 biases against those higher energy orbitals with the denominator penalty in Eq. 8.

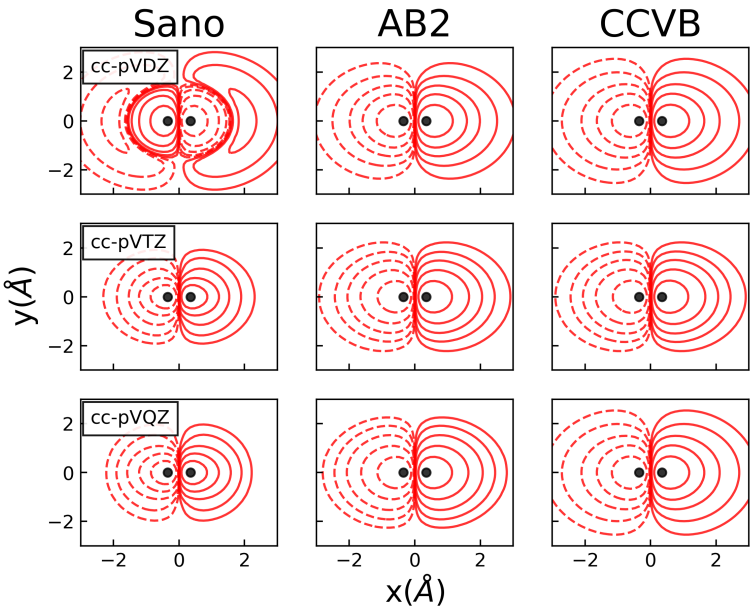

Figure 2: Comparison of σ^* orbitals predicted by Sano, AB2, and CCVB in H_2 with increasing size of the basis set. For this problem, CCVB is identical with (2,2) CASSCF. Orbitals were plotted with 10 contour isovalues logarithmically spaced [0.1,10], 5 for each phase.

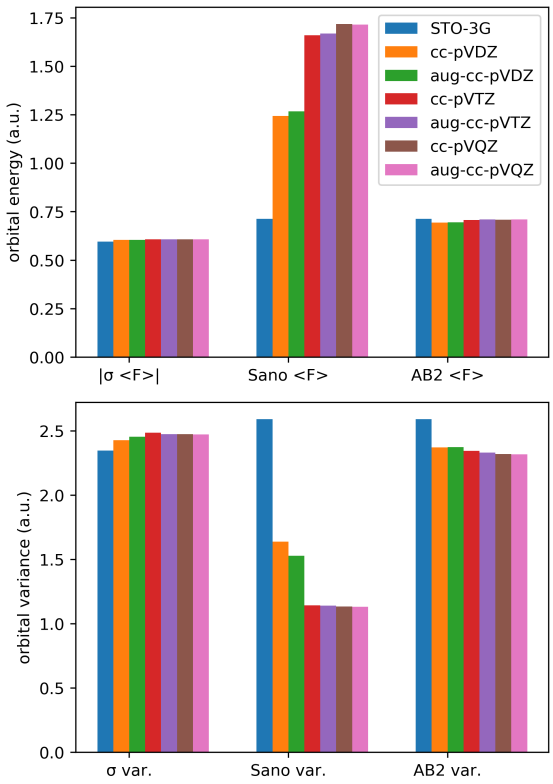

Figure 3: Comparison of orbital energy (diagonal matrix element of the Fock operator) for σ, Sano, and AB2 orbitals for H_2 with increasing size of the basis set. Bottom graph compares the variance.

Next we look into C_2H_4, where the localization scheme of Boys produces mixed $\sigma - \pi$ orbitals (sometimes called banana bonds), while Pipek-Mezey predicts separate σ and π orbitals. We will therefore use Pipek-Mezey orbitals whenever we encounter π orbitals. Inspecting the σ C-C bond in C_2H_4 in Fig. 4 shows that the shape of the occupied Pipek-Mezey and converged CCVB bonding orbitals both do not change much upon increasing the size of the basis set. By contrast, when looking at σ^* in Fig. 4 we see even poorer behaviour of the Sano C-C antibonding orbital as a function of basis set size than we did for H_2. This is confirmed in Fig. 5 where we compare the orbital energy and the orbital variance of the bonding and the antibonding C-C σ orbital in C_2H_4. The Sano σ^* orbital does not converge with the size of the basis set, with the variance decreasing, and the energy increasing. By contrast, the AB2 σ^* orbital converges rapidly both in terms of energy and variance for similar reasons to before.

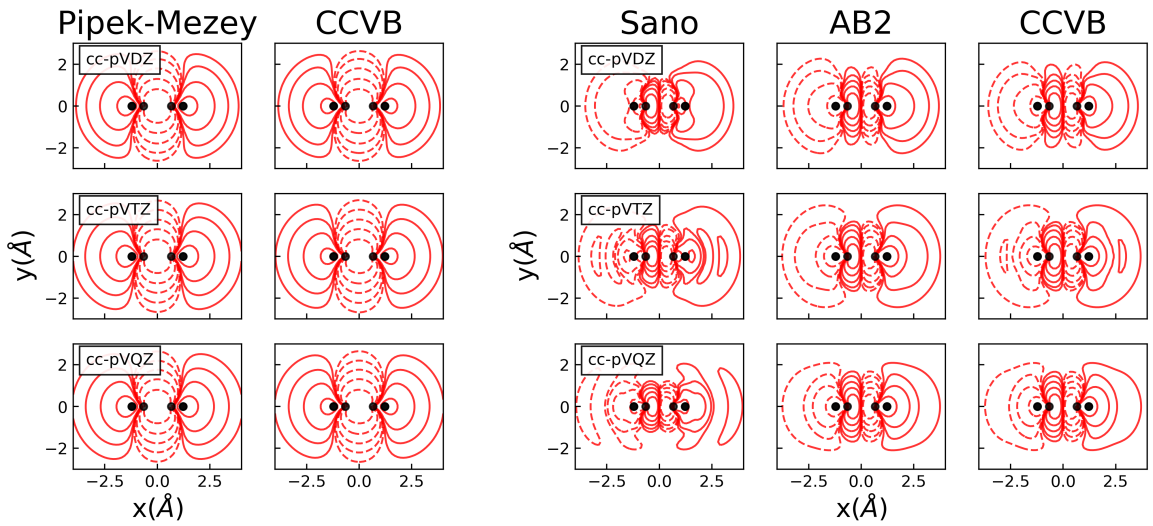

Figure 4: Comparison of σ orbitals predicted by Pipek-Mezey localization with those found by converging CCVB (top row) and σ^* orbitals predicted by Sano, AB2, and CCVB (bottom row) in C_2H_4 with increasing size of the basis set. Orbitals were plotted with 10 contour isovalues logarithmically spaced [0.1,10], 5 for each phase.

In Fig. 5 we compare the orbital energy and the orbital variance of the bonding and the antibonding orbitals for the C-C π in C_2H_4. The shortcomings of Sano seem to be much less severe in π^* orbitals. We believe this is due to the diffuse nature of the π orbitals making the maximum exchange, thus spatial locality, sufficient to describe the π^*. However, we can still see that the orbital energy and variance do not converge for Sano while they do for AB2, and converge to drastically different orbital energy and orbital variance.

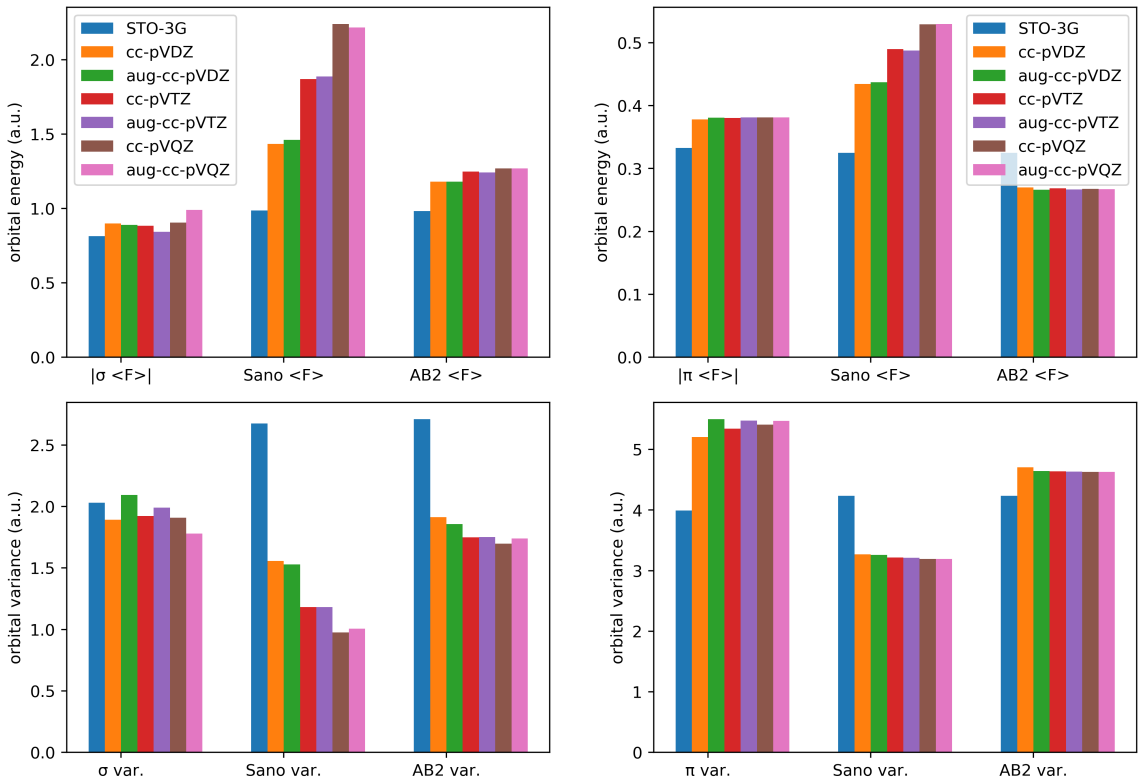

Figure 5: Comparison of orbital energy (diagonal matrix element of the Fock operator) for the C-C σ orbital with the σ^* (left) and π orbital with the π^* (right) predicted by Sano and AB2 in C_2H_4 with increasing the size of the basis set. It can be seen that Sano orbitals do not converge with increasing the basis set cardinality whereas AB2 converges much quicker especially for the σ orbital. Bottom graphs compare the spatial variance for the same orbitals where Sano contracts orbitals further with increasing the basis set, less so for the π orbital.

The quantitative advantage of the AB2 antibonding orbitals relative to the Sano orbitals seen so far can also become qualitative advantages in systems with more complex electronic structure. One such example is Cu_2, which, considering that the valence state of Cu can be taken as $3d^{10}4s^1$, is isoelectronic to H_2. The σ orbital (HOMO) of Cu_2 is shown in the upper panel of Fig. 6, along with the optimized correlating orbital from CCVB, as well as the Sano and AB2 antibonding orbitals. Maximizing exchange results in a Sano antibonding orbital that resembles an empty π-bond between the two metals. By contrast, the AB2 and CCVB orbitals look qualitatively identical.

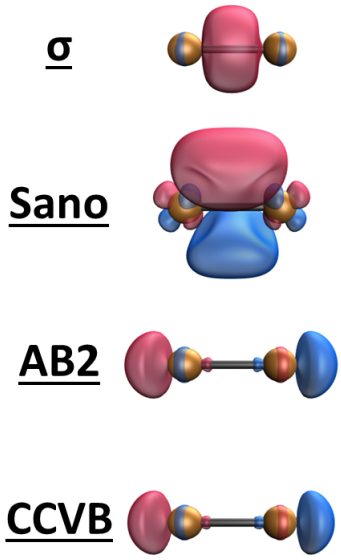

Figure 6: Comparison of the shape of the orbitals in Cu_2 where the σ bond is used to produce Sano and AB2 antibonding orbitals. While the AB2 method produces very similar orbitals to CCVB, the Sano approach fails to give a qualitatively correct antibonding orbital.

3.2 CCVB iterations

The CCVB method is a simple low-scaling approximation[49–51] to exponentially scaling spin-coupled valence bond theory that can separate a system of $2n$ electrons into fragments with spin purity, provided that UHF can also reach the dissociation limit. One price to be paid for these advantages is a challenging orbital optimization problem: the CCVB orbitals have no invariances to rotations within the active space, in contrast to CASSCF. Hence a good initial guess is very important. Sano orbitals[28] have been commonly as a starting guess for valence bond methods[51,95] such as CCVB due to their resemblance to antibonding orbitals. For simple alkanes, we examine how many iterations are needed to converge a CCVB calculation with Sano and compare with AB2 shown in Fig. 7 with increasing the molecule size and the basis set size (using the Dunning cc-pVXZ sequence of basis sets[93]). Since the double-*zeta* basis set does not involve many high energy orbitals, both methods converge almost at the same speed. Upon increasing the size of the basis set, overly-contracted Sano orbitals deviate more from the optimal antibonding orbitals, and therefore require far more iterations to converge. For this reason, we recommend using AB2 orbitals as a starting guess for valence bond methods instead of the Sano orbitals.

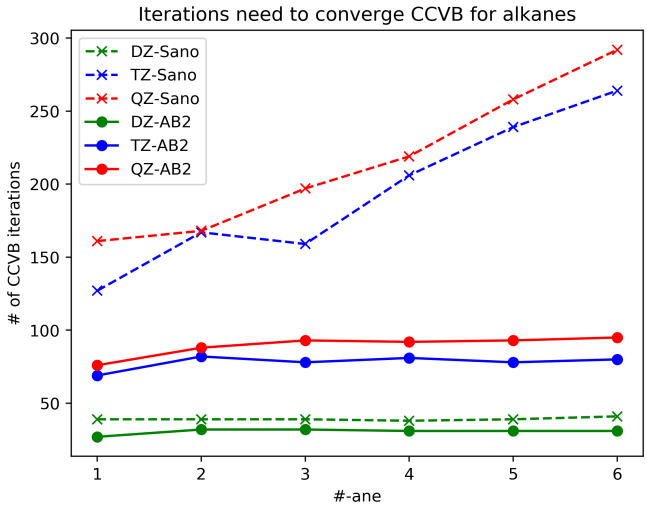

Figure 7: Number of iterations needed to converge CCVB calculations on alkanes of increasing size, with increasing ζ of the basis set. This shows a relatively constant number of iterations needed for AB2 regardless of system size, while the number of iterations rise unfavorably for the Sano guess in large basis sets. Geometric direct minimization (GDM)[95,96] is used to determine the steps.

3.3 CAS methods

The relative fraction of correlation energy recovered using AB2, Sano, FNO or other choices for antibonding orbitals to complete an active space can help us discern which ones are most appropriate to use for configuration interaction with fixed orbitals, as well as for a CASSCF initial guess. As a simple example, we stretch the C-C bond in C_2H_4 while keeping the geometry of the methylene groups fixed at those of the equilibrium ground state geometry of ethene. Looking at Fig. 8, we see that canonical virtual orbitals capture less and less correlation as the def2 basis set is improved from SVP to TZVPP to QZVPP. We also observe that the gap between Sano and AB2 orbitals increases with increasing the size of the basis set. Finally, we can see that FNO and AB2 orbitals perform almost identically and are the best choices, with AB2 having lower compute costs. Nonetheless, it is encouraging that both follow the CASSCF energies closely.

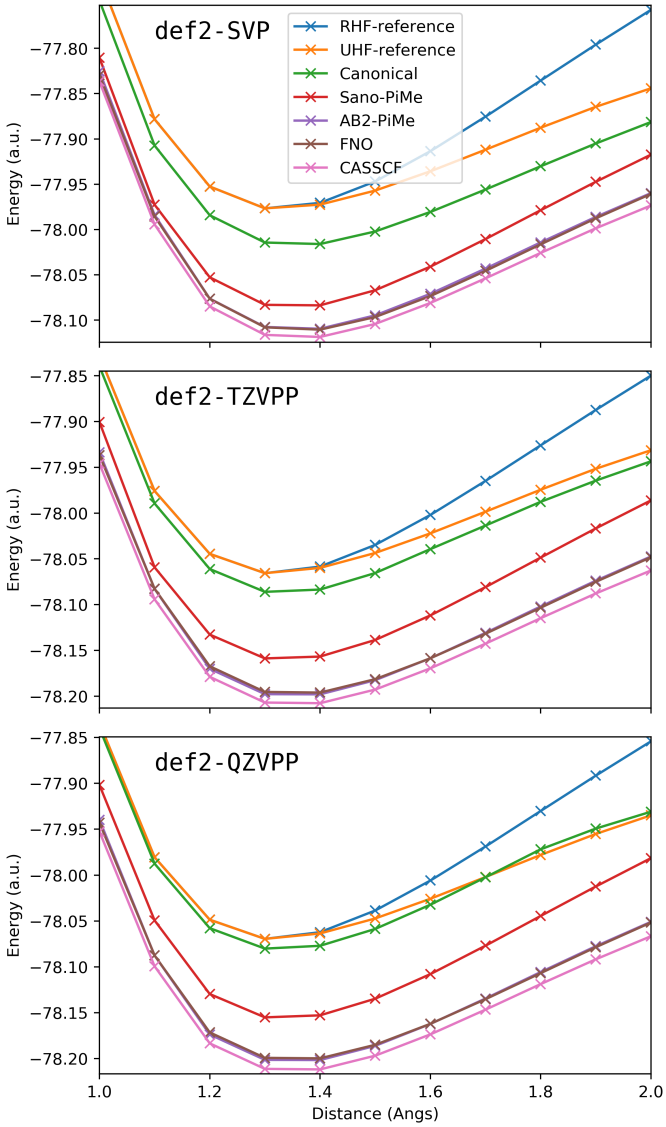

Figure 8: CAS-CI (12e,12o) for C_2H_4 using canonical, Sano, AB2, and frozen natural orbitals in three different basis sets. Restricted HF (RHF) and Unrestricted HF (UHF) curves without any correlation correction are shown for comparison.

Since the AB2 and FNO orbitals seem to capture quite a lot of the static correlation, we sought to compare them to CASSCF orbitals. In Fig. 9 we are comparing the smallest singular value of the overlap matrix between the CASSCF orbitals and those of canonical, Sano, AB2, and FNO, at the optimized geometry of C_2H_4. Once again, the canonical orbitals become dramatically worse with increasing the basis set size. Sano and FNO both become very slightly worse with increasing the size of the basis set, namely by increasing *zeta*, while AB2 seems to be nearly basis set-independent.

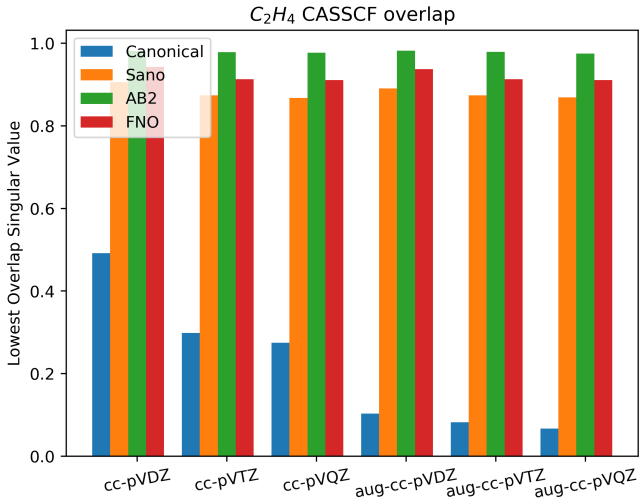

Figure 9: The smallest singular value from the overlap of CASSCF (12e,12o) orbitals with those from Sano, AB2, FNO and canonical orbitals. Canonical orbitals with the lowest energy and FNOs with the highest occupancy were selected. Canonical orbitals are differ strongly from optimized CASSCF orbitals while AB2 orbitals have the highest agreement.

3.4 Excited States

Since the AB2 orbitals seem to be good guesses for GVB methods, and yield orbitals close to converged CASSCF orbitals, this led us to believe that they could also provide a good description of valence excited states. State-specific methods, such as orbital-optimized DFT (OO-DFT)[97] need a suitable starting guess, as convergence is typically to the nearest stationary point.,[98] so we used Sano and AB2 guesses for the $\pi \rightarrow \pi^*$ excitation in methanal (H_2CO). For our purposes we employed the square gradient minimization method[98] which looks for saddle points in the orbital Hilbert space to converge restricted open-shell Kohn-Sham (ROKS).[97,99,100] In Fig. 10 we compare the overlap of the π^* orbital from converged singlet open shell HF calculations with Sano and AB2 orbitals. For this excitation, AB2 orbitals overlap the optimized orbital by at least 0.9, and vary minimally with the size of the basis set. We note here that aside from the double-*zeta* case, converging the excited state starting from the Sano orbital sometimes lands on a Rydberg excited state, while AB2 landed on the correct π^* state in all cases.

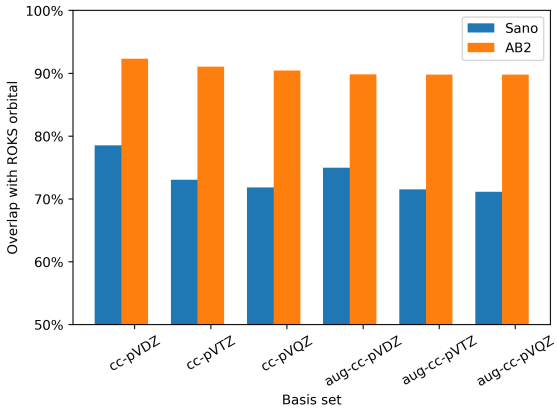

Figure 10: The overlap of the converged ROKS-HF antibonding orbital with the Sano and AB2 initial guesses in H_2CO for the $\pi \rightarrow \pi^*$ excitation. The π^* orbital is well described by AB2 regardless of basis set size.

3.5 Population Analysis

Antibonding orbitals belong to the valence space, and contribute to making a minimal basis that can be used to gain insight into chemistry, for instance via population analysis to assign effective charges on each atom. The population analysis we present here is constructed from the union of the occupied space and the antibonding orbitals without dependence on the basis set used. To study our atomic charge predictions and compare it to some other methods in the literature, we look into fluoro- and chloro-substituted methanes which have been studied theoretically[101–103] and experimentally.[104,105] These simple systems are nonetheless interesting because they manifest the effect of substituting electron withdrawing halogen atoms of different sizes and electronegativities for hydrogen in methane. How consistent or inconsistent are different atomic population analysis schemes as descriptors of these chemical substitutions?

In Fig. 11 we examine the effect of progressive substitution of hydrogen by chlorine and fluorine in the methane molecule on the computed net charge at the C atom. We consider some commonly used methods, specifically charges on electrostatic potential grid (ChElPG),[106] iterative Hirshfeld (Iter-Hirsh),[107,108] intrinsic atomic orbitals (IAO),[109,110] and the method presented in this work, molecular atomic orbitals (MAO). Most obviously, the charge transferred upon halogen substitution will depend strongly on the electronegativity difference between X and H. Furthermore, while halogens are more electronegative than hydrogen (or carbon), the electron donating capacity of C is not unlimited, and so we expect the first halogen substituted to pull away a greater fraction of an electron from C compared

to the next, and so forth. Such a change will also have some dependence on the X vs H electronegativity difference. With these preambles aside, atomic charges are not observables and therefore no single answer should be viewed as strictly correct. Nevertheless, we can examine the results of each population analysis for signs of *incorrectness* relative to physical intuition.

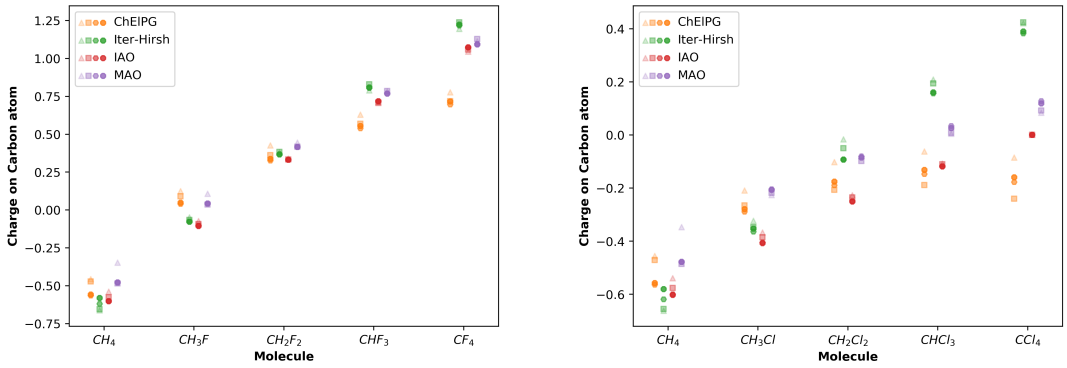

Figure 11: The charge on the carbon atom for successive chlorination and fluorination of methane predicted using four different population analysis methods (see text for the names). The triangle, square, hexagon, and octagon correspond to charges using def2-SV(P), def2-SVPD, def2-TZVPD, and def2-QZVPD, respectively.

For instance, while all methods agree that the C−H bonds of CH_4 are polarized $C^{\delta-}H^{\delta+}$, and all likewise agree that the C−F bonds of CF_4 are polarized $C^{\delta+}F^{\delta-}$, different methods predict different polarities for the C−Cl bond in CCl_4. Perhaps the most counterintuitive result is that the population on C becomes more negative via ChElPG upon going from $CHCl_3$ to CCl_4 despite the higher electronegativity of Cl vs H. At the other extreme, iterative Hirshfeld suggests that the change in C population with successive halogenation is linear, as if the electron-donating capacity of C does not saturate. This is especially striking for chlorination, and we suspect, as unreasonable as the ChElPG result for CCl_4. By contrast, we find no obvious fault with the MAO values, or with the IAO values for these interesting test cases, although we prefer the slight negative charge for Cl in CCl_4 predicted by MAO (recalling the electronegativity of chlorine is 3.5 versus carbon at 2.5 on the Pauling scale) relative to the slight positive charge predicted by IAO.

Finally we examine an unusual linear molecule, which is the result of insertion of Be into HCl, yielding H−Be−Cl.[111,112] While H−Cl is polarized as $H^{\delta+}Cl^{\delta-}$, Be has lower electronegativity than H, and so there will be substantial charge transfer. Indeed the ionic limit would be $H^-Be^{2+}Cl^-$. What then, is the actual charge distribution when we consider the covalent character of the molecular orbitals? The calculated populations are shown in Fig.

12, and it is immediately evident that predicted charges on Be vary widely. The least polar picture comes from ChElPG and MAO, with q(Be)≈+0.5, while the IAO scheme suggests q(Be)≈+1.35. How should we understand this dramatic difference and suggest which might be more correct?

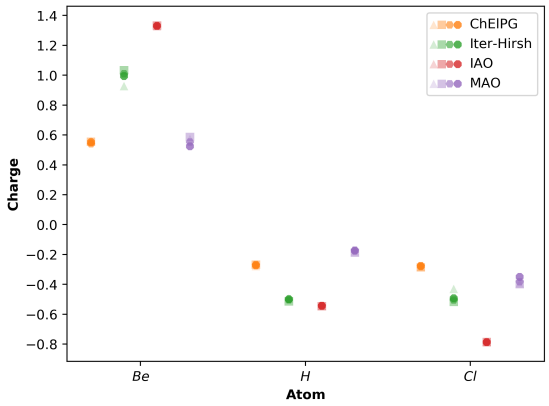

Figure 12: The charges on each atom in the BeHCl molecule predicted by the four methods mentioned in the text. The triangle, square, hexagon, and octagon correspond to charges using def2-SV(P), def2-SVPD, def2-TZVPD, and def2-QZVPD, respectively.

From the MAO perspective, there are two σ bonds involving Be, one with H and one with Cl. Each is made from *sp* hybrid orbitals on Be, meaning that the p orbitals of Be are at play in this σ bonding, as shown in Fig. 13. These bonds are both polarized away from Be, as expected. The origin of the much larger IAO charge can now be understood. The IAO reference minimal basis set, known as 'MINAO',[109] does not include 2p orbitals for Be, and therefore we are instead seeing essentially only the Be(2s) charge via the IAO approach! Iterative Hirshfeld evidently struggles with a similar issue, leading to similar overestimation of Be charge. Overall, this case nicely illustrates the advantages of the MAO population scheme that is based entirely on the system at hand, rather than some reference atomic orbitals or states.

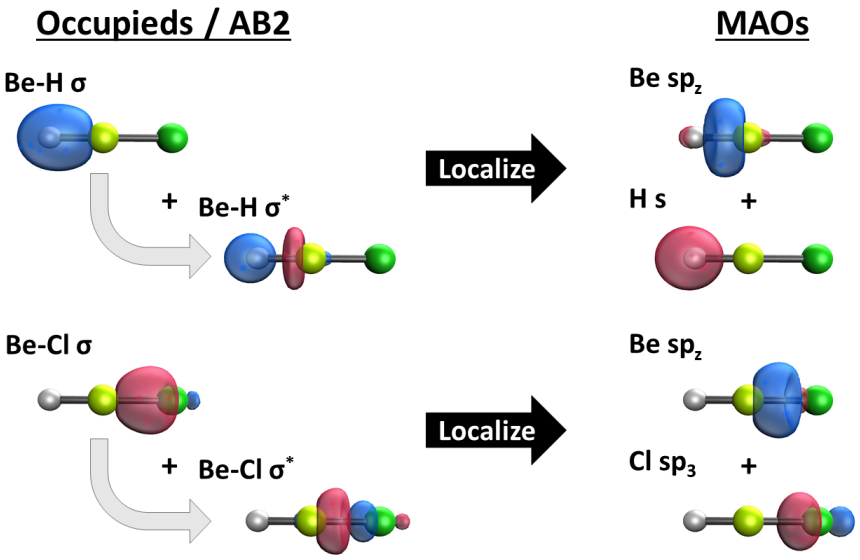

Figure 13: The union of the Boys localized bonding orbitals and their AB2 counterparts in BeHCl forms a complete valence space. Performing a Boys localization on this set of valence orbitals leads to molecule-adapted atomic orbitals that are intuitive and centered on atoms, which can then be used for population analysis.

Next we study the hypervalent molecule, SF_6, which has O_h symmetry, and whose chemical bonding has long been of interest.[113] While empty 3d functions on sulfur are needed to form 6 equivalent sp^3d^2 hybrids, the energetic cost of promoting electrons to the 3d shell is too high for d-orbital participation in the bonding to be chemically important.[46,114–117] Rather, the bonding may be thought of as resonance between Lewis structures with 4 covalent S-F bonds, and 2 F^- anions, with a formal charge of +2 on S.[118] Using Boys localization produces 6 equivalent σ_{SF} orbitals, as shown at the left of Fig. 14. As expected, these σ_{SF} bonds are strongly polarized towards the more electronegative fluorine atom. The AB2 antibonding orbitals, also shown on the left of Fig. 14 are fascinating because contrary to simple chemical expectations, they are not strongly polarized towards the sulfur atom.

Localizing the union of bonding and antibonding sets produces atom-centered MAOs, where the sulfur valence orbitals are a set of 6 equivalent orbitals that are strongly polarized towards the fluorine atoms, as shown in the third image of Fig. 14. These 6 functions are linearly independent (though non-orthogonal), and combine with the conventional hybrid orbital on each F to form the strongly polarized σ_{SF} orbitals. This hypervalent bonding problem is treated very naturally by the MAO analysis, while a minimal basis is insufficient to describe the occupied space since one in principle needs a set of 6 sp orbitals on sulfur. As measures of polarity, the calculated charges on S are +2.9 (IAO), +2.1 (Iter-Hirsh), and +1.6 (MAO) in the def2-QZVPPD basis set. The IAO charge may overestimate the polarity

due to its minimal basis on S, while the MAO charge surely underestimates it, because the MAO orbital assigned to S is actually quite strongly polarized towards F. So while the MAOs themselves provide interesting chemical insight, they cannot resolve intrinsic limitations of population analysis.

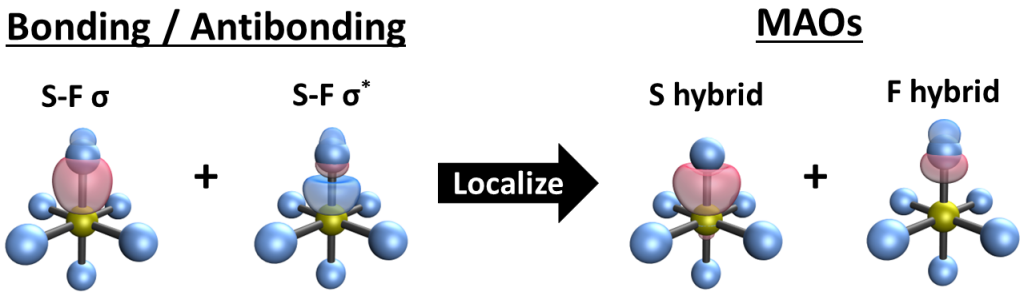

Figure 14: The union of the localized σ_{SF} bonding orbitals and the corresponding AB2 σ^*_{SF} antibonding orbitals in SF_6 forms a complete valence space describing the SF bonds (and excluding the F lone pairs). Localizing the set of valence orbitals leads to 6 molecule-adapted atomic orbitals on S (one is illustrated), showing no visual signs of d orbital participation.

There are some limitations associated with reducing the union of the localized occupied orbitals and the AB2 antibonding orbitals to a set of MAOs that should be mentioned. First, some conjugated π systems, such as benzene and $C_5H_5^-$, present a multiple minimum solution problem for orbital localization methods. Since our method relies on the localization procedure heavily, we expect there will be inconsistencies in these systems. For example, in benzene, there are different sets of solutions for the localized π orbitals, nominally corresponding to the two different Kekule structures. Using the Boys localized orbitals yields populations that reflect D_{6H} symmetry, while the Pipek-Mezey scheme gives alternating charges on successive carbons going around the ring. There is a second class of molecules that are inaccessible in our method. These are anions where the natural valence minimal basis is too small to provide an antibonding orbital for each bonding orbital. One such example is $C_5H_5^-$, the cyclopentadienyl anion. Forming the set of AB2 valence orbitals and taking the union with the occupied space leads to a set of orbitals that cannot be localized to atoms. Broadly, we can say that neutral species with a single Lewis structure are well-handled by the approach described here; as well as some more complex bonding situations like SF_6 discussed above.

4 Conclusion

We presented a relatively cheap, non-iterative procedure to produce a set of antibonding orbitals that vary minimally with the size of the atomic orbital basis set from which they are constructed. Specifically, antibonding second order (AB2) orbitals show far less variation with basis than the Sano orbitals which are sometimes used as valence antibonding orbitals. We showed that use of AB2 rather than Sano orbitals as initial guesses provides improved convergence for valence bond methods (specifically CCVB), as well as for CASSCF. The AB2 orbitals were successfully used as guesses for state-specific ROKS calculations of excited states, where they better resemble the converged orbitals than does the corresponding Sano orbital guess. We have shown how these AB2 orbitals can be used with the localized occupied orbitals to construct an effective minimal basis that can be used for population analysis among other things. Population analysis on the substituted fluormethane and chloromethane sequence shows the method is stable and consistent with other common methods that accord with chemical intuition. For the insertion of Be into HCl, the resulting charges show some advantages. Overall, the AB2 antibonding orbitals are relatively efficient to compute and quite useful for a variety of applications in quantum chemistry.

Supplementary Material

See the supplementary material for data used to generate the plots as well as the molecular geometries.

Acknowledgment

The authors would like to acknowledge support from the U.S. National Science Foundation through Grant CHE-CHE-1955643, with additional support from Q-Chem Inc. through an NIH SBIR subcontract (Grant 2R44GM121126-02). We would like to thank Prof. Farnaz Heidar-Zadeh and Dr. Susi Lehtola for very interesting discussions about localization and population analysis. MHG is a part-owner of Q-Chem Inc., which produces the software into which the developments reported here were implemented.

Data Availability

The data that supports the findings of this study are available within the article and its supplementary material.

References

(1) Szabo, A.; Ostlund, N. L. *Modern Quantum Chemistry: Introduction to Advanced Electronic Structure Theory*; Dover Publications, 1996.

(2) Jensen, F. *Angew. Chemie Int. Ed.*, 2nd ed.; Wiley, 2007; p 624.

(3) Echenique, P.; Alonso, J. L. A mathematical and computational review of Hartree-Fock SCF methods in quantum chemistry. *Mol. Phys.* **2007**, *105*, 3057–3098.

(4) Kohn, W.; Becke, A. D.; Parr, R. G. Density functional theory of electronic structure. *J. Phys. Chem.* **1996**, *100*, 12974–12980.

(5) Parr, R. G.; Yang, W. *Density-Functional Theory of Atoms and Molecules*; Oxford University Press, 1989.

(6) Burke, K.; Wagner, L. O. DFT in a nutshell. *Int. J. Quantum Chem.* **2013**, *113*, 96–101.

(7) Mardirossian, N.; Head-Gordon, M. Thirty years of density functional theory in computational chemistry: An overview and extensive assessment of 200 density functionals. *Mol. Phys.* **2017**, *115*, 2315–2372.

(8) Pulay, P. Localizability of dynamic electron correlation. *Chem. Phys. Lett.* **1983**, *100*, 151–154.

(9) Saebo, S.; Pulay, P. Local Treatment of Electron Correlation. *Annu. Rev. Phys. Chem.* **1993**, *44*, 213–236.

(10) Maslen, P. E.; Ochsenfeld, C.; White, C. A.; Lee, M. S.; Head-Gordon, M. Locality and sparsity of Ab initio one-particle density matrices and localized orbitals. *J. Phys. Chem. A* **1998**, *102*, 2215–2222.

(11) Subotnik, J. E.; Dutoi, A. D.; Head-Gordon, M. Fast localized orthonormal virtual orbitals which depend smoothly on nuclear coordinates. *J. Chem. Phys.* **2005**, *123*.

(12) Aquilante, F.; Bondo Pedersen, T.; Sánchez de Merás, A.; Koch, H. Fast noniterative orbital localization for large molecules. *J. Chem. Phys.* **2006**, *125*, 174101.

(13) Schmidt, M. W.; Hull, E. A.; Windus, T. L. Valence Virtual Orbitals: An Unambiguous ab Initio Quantification of the LUMO Concept. *J. Phys. Chem. A* **2015**, *119*, 10408–10427.

(14) Reed, A. E.; Weinhold, F. Natural bond orbital analysis of near-Hartree-Fock water dimer. *J. Chem. Phys.* **1983**, *78*, 4066–4073.

(15) Reed, A. E.; Curtiss, L. A.; Weinhold, F. Intermolecular Interactions from a Natural Bond Orbital, Donor—Acceptor Viewpoint. *Chem. Rev.* **1988**, *88*, 899–926.

(16) Fukui, K. Role of frontier orbitals in chemical reactions. *Science (80-.).* **1982**, *218*, 747–754.

(17) Fukui, K. The Role of Frontier Orbitals in Chemical Reactions (Nobel Lecture). 1982.

(18) Hoffmann, R. Building Bridges Between Inorganic and Organic Chemistry (Nobel Lecture). 1982.

(19) Khaliullin, R. Z.; Bell, A. T.; Head-Gordon, M. Electron donation in the water-water hydrogen bond. *Chem. - A Eur. J.* **2009**, *15*, 851–855.

(20) Hurley, A. C.; Lennard-Jones, J. E. The molecular orbital theory of chemical valency XIV. Paired electrons in the presence of two unlike attracting centres. *Proc. R. Soc. London. Ser. A. Math. Phys. Sci.* **1953**, *218*, 327–333.

(21) Lee, M. S.; Head-Gordon, M. Polarized atomic orbitals for self-consistent field electronic structure calculations. *J. Chem. Phys.* **1997**, *107*, 9085–9095.

(22) Iwata, S. Valence type vacant orbitals for configuration interaction calculations. *Chem. Phys. Lett.* **1981**, *83*, 134–138.

(23) Sayfutyarova, E. R.; Sun, Q.; Chan, G. K.-L. L.; Knizia, G. Automated Construction of Molecular Active Spaces from Atomic Valence Orbitals. *J. Chem. Theory Comput.* **2017**, *13*, 4063–4078.

(24) Derricotte, W. D.; Evangelista, F. A. Localized Intrinsic Valence Virtual Orbitals as a Tool for the Automatic Classification of Core Excited States. *J. Chem. Theory Comput.* **2017**, *13*, 5984–5999.

(25) Wang, Q.; Zou, J.; Xu, E.; Pulay, P.; Li, S. Automatic Construction of the Initial Orbitals for Efficient Generalized Valence Bond Calculations of Large Systems. *J. Chem. Theory Comput.* **2018**, *15*, 141–153.

(26) Lee, M. S.; Head-Gordon, M. Extracting Polarized Atomic Orbitals from Molecular Orbital Calculations. *Int. J. Quantum Chem.* **2000**, *76*, 169–184.

(27) Laikov, D. N. Intrinsic minimal atomic basis representation of molecular electronic wavefunctions. *Int. J. Quantum Chem.* **2011**, *111*, 2851–2867.

(28) Sano, T. Elementary Jacobi rotation method for generalized valence bond perfect-pairing calculations combined with simple procedure for generating reliable initial orbitals. *J. Mol. Struct. THEOCHEM* **2000**, *528*, 177–191.

(29) Foster, J. M.; Boys, S. F. Canonical Configurational Interaction Procedure. *Rev. Mod. Phys.* **1960**, *32*, 300–302.

(30) Yang, J.; Kurashige, Y.; Manby, F. R.; Chan, G. K. L. Tensor factorizations of local second-order Møller–Plesset theory. *J. Chem. Phys.* **2011**, *134*, 044123.

(31) Kurashige, Y.; Yang, J.; Chan, G. K.; Manby, F. R. Optimization of orbital-specific virtuals in local Mller-Plesset perturbation theory. *J. Chem. Phys.* **2012**, *136*, 124106.

(32) Yang, J.; Chan, G. K. L.; Manby, F. R.; Schütz, M.; Werner, H. J. The orbital-specific-virtual local coupled cluster singles and doubles method. *J. Chem. Phys.* **2012**, *136*, 144105.

(33) Neese, F.; Hansen, A.; Liakos, D. G. Efficient and accurate approximations to the local coupled cluster singles doubles method using a truncated pair natural orbital basis. *J. Chem. Phys.* **2009**, *131*.

(34) Neese, F.; Wennmohs, F.; Hansen, A. Efficient and accurate local approximations to coupled-electron pair approaches: An attempt to revive the pair natural orbital method. *J. Chem. Phys.* **2009**, *130*.

(35) Riplinger, C.; Neese, F. An efficient and near linear scaling pair natural orbital based local coupled cluster method. *J. Chem. Phys.* **2013**, *138*, 34106.

(36) Hampel, C.; Werner, H. J. Local treatment of electron correlation in coupled cluster theory. *J. Chem. Phys.* **1996**, *104*, 6286–6297.

(37) Schütz, M.; Hetzer, G.; Werner, H. J. Low-order scaling local electron correlation methods. I. Linear scaling local MP2. *J. Chem. Phys.* **1999**, *111*, 5691–5705.

(38) Schütz, M.; Werner, H. J. Low-order scaling local electron correlation methods. IV. Linear scaling local coupled-cluster (LCCSD). *J. Chem. Phys.* **2001**, *114*, 661–681.

(39) Roos, B. O.; Taylor, P. R.; Sigbahn, P. E. A complete active space SCF method (CASSCF) using a density matrix formulated super-CI approach. *Chem. Phys.* **1980**, *48*, 157–173.

(40) Ruedenberg, K.; Schmidt, M. W.; Gilbert, M. M.; Elbert, S. T. Are atoms intrinsic to molecular electronic wavefunctions? I. The FORS model. *Chem. Phys.* **1982**, *71*, 41–49.

(41) Siegbahn, P. E.; Almlöf, J.; Heiberg, A.; Roos, B. O. The complete active space SCF (CASSCF) method in a Newton-Raphson formulation with application to the HNO molecule. *J. Chem. Phys.* **1981**, *74*, 2384–2396.

(42) Roos, B. O. *Ab Initio Methods Quantum Chem. - II*; 2007; Vol. 69; pp 399–445.

(43) Cooper, D. L.; Gerratt, J.; Raimondi, M. Spin-coupled valence bond theory. *Int. Rev. Phys. Chem.* **1988**, *7*, 59–80.

(44) Cooper, D. L.; Gerratt, J.; Raimondi, M. Applications of Spin-Coupled Valence Bond Theory. *Chem. Rev.* **1991**, *91*, 929–964.

(45) Gerratt, J.; Cooper, D. L.; Karadakov, P. B.; Raimondi, M. Modern valence bond theory. *Chem. Soc. Rev.* **1997**, *26*, 87.

(46) Dunning, T. H.; Xu, L. T.; Cooper, D. L.; Karadakov, P. B. Spin-coupled generalized valence bond theory: New perspectives on the electronic structure of molecules and chemical bonds. 2021; `https://pubs.acs.org/doi/abs/10.1021/acs.jpca.0c10472`.

(47) Goddard, W. A.; Dunning, T. H.; Hunt, W. J.; Hay, P. J. Generalized Valence Bond Description of Bonding in Low-Lying States of Molecules. *Acc. Chem. Res.* **1973**, *6*, 368–376.

(48) Cullen, J. Generalized valence bond solutions from a constrained coupled cluster method. *Chem. Phys.* **1996**, *202*, 217–229.

(49) Small, D. W.; Head-Gordon, M. Tractable spin-pure methods for bond breaking: Local many-electron spin-vector sets and an approximate valence bond model. *J. Chem. Phys.* **2009**, *130*, 84103.

(50) Small, D. W.; Head-Gordon, M. Post-modern valence bond theory for strongly correlated electron spins. *Phys. Chem. Chem. Phys.* **2011**, *13*, 19285.

(51) Small, D. W.; Lawler, K. V.; Head-Gordon, M. Coupled cluster valence bond method: Efficient computer implementation and application to multiple bond dissociations and strong correlations in the acenes. *J. Chem. Theory Comput.* **2014**, *10*, 2027–2040.

(52) Lehtola, S.; Parkhill, J.; Head-Gordon, M. Orbital optimisation in the perfect pairing hierarchy: applications to full-valence calculations on linear polyacenes. *Mol. Phys.* **2018**, *116*, 547–560.

(53) Stück, D.; Baker, T. A.; Zimmerman, P.; Kurlancheek, W.; Head-Gordon, M. On the nature of electron correlation in C60. *J. Chem. Phys.* **2011**, *135*, 194306.

(54) Ibeji, C. U.; Ghosh, D. Singlet-triplet gaps in polyacenes: A delicate balance between dynamic and static correlations investigated by spin-flip methods. *Phys. Chem. Chem. Phys.* **2015**, *17*, 9849–9856.

(55) Boys, S. F. Construction of Molecular orbitals to be minimally variant for changes from one molecule to another. *Rev. Mod. Phys.* **1960**, *32*, 296–299.

(56) Edmiston, C.; Ruedenberg, K. Localized atomic and molecular orbitals. *Rev. Mod. Phys.* **1963**, *35*, 457–464.

(57) Pipek, J.; Mezey, P. G. A fast intrinsic localization procedure applicable for ab initio and semiempirical linear combination of atomic orbital wave functions. *J. Chem. Phys.* **1989**, *90*, 4916–4926.

(58) Huzinaga, S.; Arnau, C. Virtual orbitals in hartree-fock theory. *Phys. Rev. A* **1970**, *1*, 1285–1288.

(59) Huzinaga, S.; Arnau, C. Virtual orbitals in hartree-fock theory. II. *J. Chem. Phys.* **1971**, *54*, 1948–1951.

(60) Bender, C. F.; Davidson, E. R. Theoretical calculation of the potential curves of the Be2 molecule. *J. Chem. Phys.* **1967**, *47*, 4972–4978.

(61) Bonaccorsi, R.; Petrongolo, C.; Scrocco, E.; Tomasi, J. Configuration-interaction calculations for the ground state of OF2, NO2-, CN-: Canonical orbitals and exclusive orbitals. *Theor. Chim. Acta* **1969**, *15*, 332–343.

(62) Wasilewski, J. Modified virtual orbitals (MVO) in limited CI calculations. *Int. J. Quantum Chem.* **1991**, *39*, 649–656.

(63) Beran, G. J. O.; Austin, B.; Sodt, A.; Head-Gordon, M. Unrestricted Perfect Pairing: The Simplest Wave-Function-Based Model Chemistry beyond Mean Field. *J. Phys. Chem. A* **2005**, *109*, 9183–9192.

(64) Lawler, K. V.; Small, D. W.; Head-Gordon, M. Orbitals that are unrestricted in active pairs for generalized valence bond coupled cluster methods. *J. Phys. Chem. A* **2010**, *114*, 2930–2938.

(65) Löwdin, P.-O. In *Adv. Chem. Phys.*; Prigogine, I., Ed.; Advances in Chemical Physics; 1958; pp 207–322.

(66) Møller, C.; Plesset, M. S. Note on an approximation treatment for many-electron systems. *Phys. Rev.* **1934**, *46*, 618–622.

(67) Head-Gordon, M.; Pople, J. A.; Frisch, M. J. MP2 energy evaluation by direct methods. *Chem. Phys. Lett.* **1988**, *153*, 503–506.

(68) Kapuy, E.; Csépes, Z.; Kozmutza, C. Application of the many-body perturbation theory by using localized orbitals. *Int. J. Quantum Chem.* **1983**, *23*, 981–990.

(69) Kapuy, E.; Bartha, F.; Bogár, F.; Csépes, Z.; Kozmutza, C. Applications of the MBPT in the localized representation. *Int. J. Quantum Chem.* **1990**, *38*, 139–147.

(70) Taube, A. G.; Bartlett, R. J. Frozen natural orbitals: Systematic basis set truncation for coupled-cluster theory. *Collect. Czechoslov. Chem. Commun.* **2005**, *70*, 837–850.

(71) Taube, A. G.; Bartlett, R. J. Frozen natural orbital coupled-cluster theory: Forces and application to decomposition of nitroethane. *J. Chem. Phys.* **2008**, *128*.

(72) Salter, E. A.; Trucks, G. W.; Fitzgerald, G.; Bartlett, R. J. Theory and application of MBPT(3) gradients: The density approach. *Chem. Phys. Lett.* **1987**, *141*, 61–70.

(73) Trucks, G. W.; Salter, E. A.; Sosa, C.; Bartlett, R. J. Theory and implementation of the MBPT density matrix. An application to one-electron properties. *Chem. Phys. Lett.* **1988**, *147*, 359–366.

(74) Frisch, M. J.; Head-Gordon, M.; Pople, J. A. A direct MP2 gradient method. *Chem. Phys. Lett.* **1990**, *166*, 275–280.

(75) Mulliken, R. S. Criteria for the construction of good self-consistent-field molecular orbital wave functions, and the significance of LCAO-MO population analysis. *J. Chem. Phys.* **1962**, *36*, 3428–3439.

(76) Mulliken, R. S. Chemical bonding. *Annu. Rev. Phys. Chem.* **1978**, *29*, 1–30.

(77) Mulliken, R. S. Electronic population analysis on LCAO-MO molecular wave functions. II. Overlap populations, bond orders, and covalent bond energies. *J. Chem. Phys.* **1955**, *23*, 1841–1846.

(78) Mulliken, R. S. Electronic population analysis on LCAO-MO molecular wave functions. I. *J. Chem. Phys.* **1955**, *23*, 1833–1840.

(79) Davidson, E. R. Electronic population analysis of molecular wavefunctions. *J. Chem. Phys.* **1967**, *46*, 3320–3324.

(80) Roby, K. R. Quantum theory of chemical valence concepts I. Definition of the charge on an atom in a molecule and of occupation numbers for electron density shared between atoms. *Mol. Phys.* **1974**, *27*, 81–104.

(81) Ruedenberg, K.; Schmidt, M. W.; Gilbert, M. M. Are atoms intrinsic to molecular electronic wavefunctions? II. Analysis of fors orbitals. *Chem. Phys.* **1982**, *71*, 51–64.

(82) Ruedenberg, K.; Schmidt, M. W.; Gilbert, M. M.; Elbert, S. T. Are atoms intrinsic to molecular electronic wavefunctions? III. Analysis of FORS configurations. *Chem. Phys.* **1982**, *71*, 65–78.

(83) Mayer, I. Non-orthogonal localized orbitals and orthogonal atomic hybrids derived from Mulliken's population analysis. *Chem. Phys. Lett.* **1995**, *242*, 499–506.

(84) Epifanovsky, E.; Gilbert, A. T. B.; Feng, X.; Lee, J.; Mao, Y.; Mardirossian, N.; Pokhilko, P.; White, A. F.; Coons, M. P.; Dempwolff, A. L. et al. Software for the frontiers of quantum chemistry: An overview of developments in the Q-Chem 5 package. *J. Chem. Phys.* **2021**, *155*, 084801.

(85) Liang, W.; Shao, Y.; Ochsenfeld, C.; Bell, A. T.; Head-Gordon, M. Fast evaluation of a linear number of local exchange matrices. *Chem. Phys. Lett.* **2002**, *358*, 43–50.

(86) Subotnik, J. E.; Shao, Y.; Liang, W. Z.; Head-Gordon, M. An efficient method for calculating maxima of homogeneous functions of orthogonal matrices: Applications to localized occupied orbitals. *J. Chem. Phys.* **2004**, *121*, 9220–9229.

(87) Subotnik, J. E.; Sodt, A.; Head-Gordon, M. Localized orbital theory and ammonia triborane. *Phys. Chem. Chem. Phys.* **2007**, *9*, 5522.

(88) Pipek, J. Localization measure and maximum delocalization in molecular systems. *Int. J. Quantum Chem.* **1989**, *36*, 487–501.

(89) Shavitt, I. *Methods Electron. Struct. Theory*; Springer, Boston, MA, 1977; pp 189–275.

(90) Siegbahn, P. E. A new direct CI method for large CI expansions in a small orbital space. *Chem. Phys. Lett.* **1984**, *109*, 417–423.

(91) Knowles, P. J.; Handy, N. C. A new determinant-based full configuration interaction method. *Chem. Phys. Lett.* **1984**, *111*, 315–321.

(92) Levine, B. G.; Durden, A. S.; Esch, M. P.; Liang, F.; Shu, Y. CAS without SCF - Why to use CASCI and where to get the orbitals. *J. Chem. Phys.* **2021**, *154*, 090902.

(93) Dunning, T. H. Gaussian basis sets for use in correlated molecular calculations. I. The atoms boron through neon and hydrogen. *J. Chem. Phys.* **1989**, *90*, 1007–1023.

(94) Weigend, F.; Ahlrichs, R. Balanced basis sets of split valence, triple zeta valence and quadruple zeta valence quality for H to Rn: Design and assessment of accuracy. *Phys. Chem. Chem. Phys.* **2005**, *7*, 3297–3305.

(95) Van Voorhis, T.; Head-Gordon, M. Implementation of generalized valence bond-inspired coupled cluster theories. *J. Chem. Phys.* **2002**, *117*, 9190–9201.

(96) Van Voorhis, T.; Head-Gordon, M. A geometric approach to direct minimization. *Mol. Phys.* **2002**, *100*, 1713–1721.

(97) Hait, D.; Head-Gordon, M. Orbital Optimized Density Functional Theory for Electronic Excited States. *J. Phys. Chem. Lett.* **2021**, *12*, 4517–4529.

(98) Hait, D.; Head-Gordon, M. Excited State Orbital Optimization via Minimizing the Square of the Gradient: General Approach and Application to Singly and Doubly Excited States via Density Functional Theory. *J. Chem. Theory Comput.* **2020**, *16*, 1699–1710.

(99) Frank, I.; Hutter, J.; Marx, D.; Parrinello, M. Molecular dynamics in low-spin excited states. *J. Chem. Phys.* **1998**, *108*, 4060–4069.

(100) Filatov, M.; Shaik, S. A spin-restricted ensemble-referenced Kohn-Sham method and its application to diradicaloid situations. *Chem. Phys. Lett.* **1999**, *304*, 429–437.

(101) Rayez, M.-T.; Rayez, J.-C.; Sawerysyn, J.-P. Ab Initio Studies of the Reactions of Chlorine Atoms with Fluoro- and Chloro-Substituted Methanes. *J. Phys. Chem.* **1994**, *98*, 11342–11352.

(102) Davis, S. R. Ab initio study of the insertion reaction of magnesium into the carbon-halogen bond of fluoro- and chloromethane. *J. Am. Chem. Soc.* **1991**, *113*, 4145–4150.

(103) Fonseca Guerra, C.; Handgraaf, J.-W.; Baerends, E. J.; Bickelhaupt, F. M. Voronoi deformation density (VDD) charges: Assessment of the Mulliken, Bader, Hirshfeld, Weinhold, and VDD methods for charge analysis. *J. Comput. Chem.* **2004**, *25*, 189–210.

(104) Sundin, S.; Saethre, L. J.; Sorensen, S. L.; Ausmees, A.; Svensson, S. Vibrational structure of the chloromethane series, CH4-nCln, studied by core photoelectron spectroscopy and ab initio calculations. *J. Chem. Phys.* **1999**, *110*, 5806–5813.

(105) Kokkonen, E.; Jänkälä, K.; Patanen, M.; Cao, W.; Hrast, M.; Bučar, K.; Žitnik, M.; Huttula, M. Role of ultrafast dissociation in the fragmentation of chlorinated methanes. *J. Chem. Phys.* **2018**, *148*, 174301.

(106) Breneman, C. M.; Wiberg, K. B. Determining atom-centered monopoles from molecular electrostatic potentials. The need for high sampling density in formamide conformational analysis. *J. Comput. Chem.* **1990**, *11*, 361–373.

(107) Hirshfeld, F. L. Bonded-atom fragments for describing molecular charge densities. *Theor. Chim. Acta* **1977**, *44*, 129–138.

(108) Bultinck, P.; Van Alsenoy, C.; Ayers, P. W.; Carbó-Dorca, R. Critical analysis and extension of the Hirshfeld atoms in molecules. *J. Chem. Phys.* **2007**, *126*, 144111.

(109) Knizia, G. Intrinsic atomic orbitals: An unbiased bridge between quantum theory and chemical concepts. *J. Chem. Theory Comput.* **2013**, *9*, 4834–4843.

(110) Senjean, B.; Sen, S.; Repisky, M.; Knizia, G.; Visscher, L. Generalization of Intrinsic Orbitals to Kramers-Paired Quaternion Spinors, Molecular Fragments, and Valence Virtual Spinors. *J. Chem. Theory Comput.* **2021**, *17*, 1337–1354.

(111) Hashimoto, K.; Osamura, Y.; Iwata, S. Ab initio study of structure and stability of beryllium compounds. *J. Mol. Struct. THEOCHEM* **1987**, *152*, 101–117.

(112) Yu, W.; Andrews, L.; Wang, X. Infrared Spectroscopic and Electronic Structure Investigations of Beryllium Halide Molecules, Cations, and Anions in Noble Gas Matrices. *J. Phys. Chem. A* **2017**, *121*, 8843–8855.

(113) Coulson, C. A. d Electrons and Molecular Bonding. *Nature* **1969**, *221*, 1106–1110.

(114) Kiang, T.; Zare, R. N. Stepwise Bond Dissociation Energies in Sulfur Hexafluoride. *J. Am. Chem. Soc.* **1980**, *102*, 4024–4029.

(115) Reed, A. E.; Weinhold, F. On the role of d orbitals in sulfur hexafluoride. *J. Am. Chem. Soc.* **1986**, *108*, 3586–3593.

(116) Cooper, D. L.; Cunningham, T. P.; Gerratt, J.; Karadakov, P. B.; Raimondi, M. Chemical Bonding to Hypercoordinate Second-Row Atoms: d Orbital Participation versus Democracy. *J. Am. Chem. Soc.* **1994**, *116*, 4414–4426.

(117) Kalemos, A. Hypervalent Bonding in the OF(a4Σ-), SF(a4Σ-), SF5/SF6, and OSF4 Species. *J. Phys. Chem. A* **2018**, *122*, 2178–2183.

(118) Jackson, B. A.; Harshman, J.; Miliordos, E. Addressing the Hypervalent Model: A Straightforward Explanation of Traditionally Hypervalent Molecules. *J. Chem. Educ.* **2020**, *97*, 3638–3646.